RESEARCH ARTICLE

International Journal of Climatology   RMetS

Summertime precipitation deficits in the southern Peruvian highlands since 1964

Noemi Imfeld[1,2] ◉ | Christian Barreto Schuler[3] | Kris Milagros Correa Marrou[3] | Martín Jacques-Coper[4,5] | Katrin Sedlmeier[2] | Stefanie Gubler[2] ◉ | Adrian Huerta[6] | Stefan Brönnimann[1]

[1]Oeschger Centre for Climate Change Research and Institute of Geography, University of Bern, Bern, Switzerland

[2]Analysis and Forecasting Division, Swiss Federal Office of Meteorology and Climatology, MeteoSwiss, Zurich, Switzerland

[3]Dirección de Meteorología y Evaluación Ambiental Atmosférica. Servicio Nacional de Meteorología e Hidrología (SENAMHI), Lima, Peru

[4]Departamento de Geofisica, Universidad de Concepción, Concepción, Chile

[5]Center for Climate and Resilience Research (CR)2, Chile

[6]Dirección de Hidrología. Servicio Nacional de Meteorología e Hidrología (SENAMHI), Lima, Peru

Correspondence
Noemi Imfeld, Swiss Federal Office of Meteorology and Climatology, MeteoSwiss, Operation Center 1, 8058 Zurich, Switzerland.
Email: noemi@imfeld.info

Abstract

Precipitation deficits remain a concern to the rural population in the southern Peruvian highlands and knowledge about their occurrence is lacking because of scarce data availability. For mountainous regions with sparse station networks, reanalyses can provide valuable information; however, known limitations in reproducing precipitation are aggravated due to unresolved topographical effects. In this study, we assess in a first step the representation of precipitation during the rainy season (January–February–March) in seven reanalysis data sets in comparison to a newly generated gridded precipitation data set for Peru. In a second step, we assess summer precipitation deficits in Peru during the second half of the 20th century.

In the reanalyses data sets, we find biases strongly influenced by the topography of the models and low correlations for the rainy season. Thus, reanalyses do not solve the problem of data scarcity for this region either. Furthermore, we confirm that El Niño is not a sufficient stratification criterion for precipitation deficits during the rainy season (JFM) in the southern Peruvian highlands. Based on observational records and reanalyses, a considerable fraction of inter-annual variability of precipitation can be explained through upper-tropospheric zonal wind anomalies. Westerly wind anomalies, often related to the warming of the troposphere during an El Niño event, lead to dry conditions, but not all El Niño events produce these westerly wind anomalies. Atmospheric simulations indicate differences between precipitation deficits in central Pacific and eastern Pacific El Niño flavours, which cannot be addressed in observations due to reduced record length: Droughts in the southern Peruvian Andes during eastern Pacific El Niño events seem to be related to a stronger warming in the troposphere above the central Pacific ocean, whereas this is not the case for droughts during central Pacific El Niño events. These results, however, need to be further corroborated by model studies and palaeoclimatological research.

KEYWORDS
drought, ENSO, ERA-20CM, mountain, Peru, rainfall, reanalysis, SPI

---

1 | INTRODUCTION

Precipitation deficits during the rainy season in austral summer (January–February–March) have been impairing local population and the agriculture sector in the southern Andes of Peru throughout the last century. For this region, summer precipitation is the main water resource, contributing to around 60% of annual precipitation, followed by spring and autumn with both around 20% (Thibeault et al., 2011; Perry et al., 2014). Especially for the agricultural sector, information about precipitation variability or monitoring of the current drought conditions is important as it enables adaptation or mitigation measures on long and short timescales. Providing such information for the agricultural sector is a goal of Climandes-2, a twinning project between the National Weather Services of Peru (SENAMHI Peru) and Switzerland (MeteoSwiss) during which the presented analyses have been performed. In this paper, we focus on the pilot regions of the project, that is, Cusco, Puno and Junin (CPJ) located in the southern Andes of Peru.

Reanalysis data sets may provide valuable information about precipitation in regions with sparse station networks such as in CPJ. In the current global reanalyses, limitations in the representation of precipitation are however common for areas with complex topography and low amounts of assimilated data (Diro et al., 2009; Blacutt et al., 2015). A systematic evaluation of reanalyses against observational data is therefore necessary. For Peru, such a systematic evaluation has not been conducted yet and a first attempt is presented in this paper.

In addition to direct information about precipitation, reanalyses provide information on the mechanisms causing precipitation or lack thereof. This information is relevant in the context of climate change scenarios, which indicate a decrease of precipitation in the central Andes for the coming century (Minvielle and Garreaud, 2011; Thibeault et al., 2011; Neukom et al., 2015). Minvielle and Garreaud (2011) and Thibeault et al. (2011) find an increase in westerly winds at 200 hPa and deducted thereof a decrease in precipitation of 10–30%. Neukom et al. (2015) shows that even under an emission scenario with strong greenhouse gas reduction, precipitation reduction in the central Andes will be outside pre-industrial natural variability. Because general circulation models (GCMs) show only limited abilities in simulating precipitation, these studies use the relationship between precipitation and upper-level winds for their projections.

The upper-level circulation is seen as a main mechanism for subseasonal, annual and inter-annual precipitation variability (Lenters and Cook, 1999; Vuille, 1999; Garreaud and Aceituno, 2001; Garreaud et al., 2003; Garreaud, 2009). Stronger easterly (westerly) winds at 200 hPa are related to wet (dry) conditions, as these upper-level winds favour (hinder) the transport of moist air from the Amazon basin (Garreaud, 1999; Falvey and Garreaud, 2005). During summertime, as a consequence of the build-up of an anticyclonic pressure system, the Bolivian High, easterly winds blow over the central Andes. However, during El Niño situations, increased westerly wind anomalies are present over the central Andes as a result of the winds being in geostrophic balance with the meridional baroclinicity caused by the warming of the troposphere (Garreaud, 2009).

Depending on the spatial pattern, temporal evolution and amplitude of anomalous sea surface temperatures (SSTs) warming, El Niño events are differentiated into three types or flavours, Eastern-Pacific El Niño (EP or canonical El Niño), Central-Pacific El Niño (CP or El Niño Modoki) and a mixed EP/CP type (Kao and Yu, 2009; Yu et al., 2012) with distinct effects on atmospheric circulation and precipitation in South America (Tedeschi et al., 2013; Tedeschi and Collins, 2016). EP events are characterized by strong surface westerly wind anomalies throughout the tropical Pacific and an eastwards shift of the ascending branch of the Walker circulation. For CP events, westerly wind anomalies are present mainly in the western and central Pacific with a more westwards location of enhanced convectivity and maximum water vapour increase compared to EP, consequently affecting patterns such as the Intertropical Convergence Zone (ITCZ) and South Pacific Convergence Zone (SPCZ; Capotondi et al., 2015; Hu et al., 2016; Andreoli et al., 2017).

Through the eastwards shift of the Walker circulation and the alteration of the winds over the central Andes, El Niño affects the mechanisms governing precipitation variability in the southern Peruvian highlands. The two El Niño indices NIÑO1+2 and NIÑO3.4 both correlate negatively with precipitation sums in the area of southern Peru during the austral summer months December, January and February (Lagos et al., 2008). Morales et al. (2012) show that precipitation reconstruction has a clear El Niño–Southern Oscillation (ENSO)-like pattern at inter-annual to multi-centennial timescales for the Altiplano of Bolivia. Seiler et al. (2013) find El Niño to lead to drier and more variable conditions in the Andes of Bolivia. For the Mantaro River basin, a region close to CPJ, dry spells are significantly more likely to occur during El Niño than La Niña (Sulca et al., 2016). For Peru, Sulca et al. (2017) find that the two indices E (eastern Pacific) and C (central Pacific) describing SST anomalies in the central and eastern Pacific (see Sulca et al., 2017 for description of the indices) are both related to weaker upper-level easterly wind over Peru and that the position of the SPCZ influences rainfall over western Peru and the Bolivian Altiplano. A separation into different flavours of El Niño is therefore important for the evaluation of drought occurrence.

In a first step, this study evaluates the abilities of different reanalyses in representing the precipitation patterns, inter-annual variability and the annual cycle in order to assess the use of reanalysis for drought monitoring. Then, we analyse the relationship between summertime precipitation and tropical Pacific SST in the reanalysis JRA-55 together with observations and climate model simulations to gain further insights about the SST–drought mechanism. We specifically look at the difference in upper-level atmospheric conditions of El Niño events (EP or CP) and how this is related to the occurrence of droughts in the southern Peruvian Andes.

Our paper is organized as follows: Section 2 explains the data sets and methods. In section 3, we present our results and discussion, and section 4 gives a conclusion of our findings.

2 | DATA AND METHODS

2.1 | Data

As a reference for the evaluation of reanalyses, we use two observational data sets: (a) monthly Peruvian-interpolated data of the SENAMHI's climatological and hydrological observations, PISCOpv2.0 (Aybar *et al.*, 2017), which is a gridded data set generated from station and satellite data, and (b) a regular observational data set from rain gauges (Figure 1a). The PISCOp data set is available at a $0.05 \times 0.05°$ resolution on a monthly basis for the period 1981–2016. The generation of PISCOp has been facing multiple constraints, such as low station density in an area with complex topography, low quality of station data and inherent biases in satellite data sets. For example in the Amazon

lowland regions, the station density is low and thus PISCOp consists mainly of CHIRPMm, a modification of CHPclim based on the climatology of TRMM2A25 (Aybar *et al.*, 2017). For CHIRPS (which already includes a station merging), a validation with reference data showed low correlation values and high bias ratios for the northern lowlands of Peru (Funk *et al.*, 2015). Nevertheless, PISCOp is the first high-resolution gridded data set for Peru, and thus, provides a valuable source of information so far not available.

The observational records are a quality controlled and homogenized data set (without gap filling) spanning the period from 1964 to present provided by SENAMHI Peru (Rosas *et al.*, 2016). For the generation of the gridded data set, a gap filled station data set has been used, containing more stations, than the herein used station data set. Thus, at stations location, station and the gridded data do not completely agree, but show correlations of 0.71–0.95 for JFM precipitation.

The evaluated reanalyses include four data sets covering the last decades: MERRA (Rienecker *et al.*, 2011), ERA-Interim (Dee *et al.*, 2011), NCEP/NCAR R1 (NNR; Kalnay *et al.*, 1996) and JRA-55 (Kobayashi *et al.*, 2015). NNR and JRA-55 are the only two reanalyses with a full assimilation system spanning the complete period of station observations, thus incorporating the satellite and pre-satellite era. NNR is evaluated despite its old model vintage as it is a widely used reanalysis for research and application in South America. Furthermore, we evaluate three surface-only reanalyses spanning the 20th century: 20CRv2c (Compo *et al.*, 2011), ERA-20C (Poli *et al.*, 2016) and CERA-20C (Laloyaux *et al.*, 2018). 20CRv2c assimilates surface pressure, while ERA-20C and CERA-20C also assimilate marine winds. CERA-20C is a coupled ocean–atmosphere reanalysis.

FIGURE 1   (a) Mean daily precipitation of JFM from PISCOp and station data for 1981–2016. Filled circles show station measurements. At station location, the gridded data set and the stations correlate with values between 0.71 and 0.95. (b) Pearson correlation for PISCOp (colours) and stations (circles) with NIÑO3.4. and with NIÑO1+2 (contours). Solid/dashed contours contours indicate significantly negative/positive correlation areas. Only significant correlations at a 95% significance level are shown. 1,000 m a.s.l shown as black contour line. Lake Titicaca is shown in the south of the Peruvia Andes [Colour figure can be viewed at wileyonlinelibrary.com]
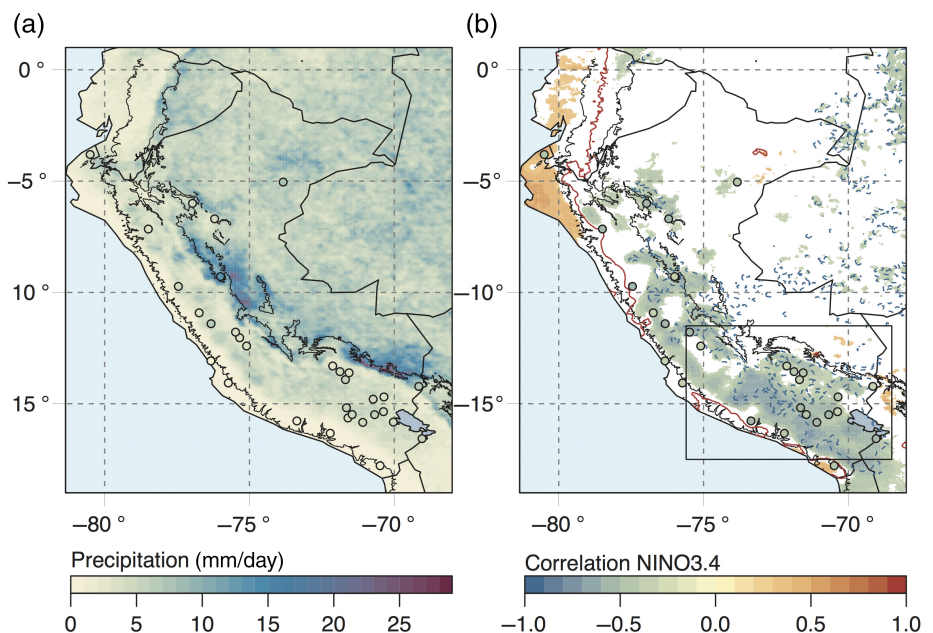
TABLE 1 List of data sets for precipitation evaluation and drought composite study

Data sets	Time period	Resolution	Scheme	Model vintage	Source
Reanalyses					
MERRA	1979–2016	0.5 × 0.667°	GEOS IAU	2009	Rienecker *et al.* (2011)
ERA-Interim	1979–2011	T255L60	4DVAR	2006	Dee *et al.* (2011)
NCEP/NCAR R1	1948–present	T62L28	3DVAR	1995	Kalnay *et al.* (1996)
JRA-55	1958–present	T319L60	4DVAR	2009	Kobayashi *et al.* (2015)
20CRv2c	1851–2014	T62L28	EnKF	2009	Compo *et al.* (2011)
ERA-20C	1901–2010	T159L91	4DVAR	2012	Poli *et al.* (2016)
CERA-20C	1900–2010	T159L137	4DVAR	2016	Laloyaux *et al.* (2018)
Model simulations					
ERA-20CM	1899–2010	T159L91		2012	Hersbach *et al.* (2015)
Observations					
Station data	1964–present				Senamhi Peru (Rosas *et al.*, 2016)
Gridded products					
PISCOP	1981–present	0.05 × 0.05°			Aybar *et al.* (2017)

ERA-20C is a single-member reanalysis, while 20CRv2c and CERA-20C are ensemble products. Specific information about all data sets is summarized in Table 1.

To explore the influence of SST on circulation and precipitation amounts in the CPJ region, we use the ERA-20CM simulations (Hersbach *et al.*, 2015). ERA-20CM is an "AMIP-type" (Atmospheric Model Intercomparison Project) model simulation with an ensemble of 10 model integrations spanning 1899–2010. The above mentioned ERA-20C reanalysis and ERA-20CM are based on the same model configuration, but ERA-20CM does not assimilate observations. Whereas ERA-20C is based on the first (m0) of 10 random drawings from the HadISST2.1.0.0 data set for boundary conditions, ERA-20CM is based on 10 realizations of SST and sea-ice cover (SIC). These realizations are considered as the most plausible SST fields and their variations reflect the uncertainty of observations in the boundary conditions in addition to the initial conditions (Titchner and Rayner, 2014). The SST data from HadISST2.1.0.0 are based on in situ SST observations and satellite data (AVHRR and retrievals of ARC-ATSR reprocessing).

For 2-m temperature, the evaluation of ERA-20CM ensemble mean and spread shows a good representation of short-term variability, such as the cooling after volcanic eruptions and warming during El Niño. De Boisséson *et al.* (2014) show that ERA-20CM captures changes in the tropical wind circulation and Hegerl *et al.* (2018) find a good representation of the Pacific Walker circulation in ERA-20CM. As the ERA-20CM model simulations are SST driven, the two results suggest the dependence of these winds on SST. In comparison, CMIP5 models generally do not allow for a year-to-year comparison (Hersbach *et al.*, 2015) and do not

capture changes in the tropical wind circulation (England *et al.*, 2014). The ERA-20CM simulations thus provide a statistical estimate of the model climate and ensemble mean and spread allow for conclusions as to the effect of boundary conditions, most importantly SST. Due to the comparability to reanalyses, the SST variations reflecting uncertainty in observational records and the good representation of El Niño short-term variability, the ERA-20CM proves to be a suitable model for the herein conducted analysis.

For a measure of El Niño, we rely on the widely applied Oceanic Niño Index (ONI) based on ERSSTv4 data (Huang *et al.*, 2015) provided by the Climate Prediction Center (CPC). In addition, we calculate correlations with the two El Niño SST indices NIÑO3.4 and NIÑO1+2 from HadISST1 data set (Rayner *et al.*, 2003).

2.2 | Evaluation of reanalyses and model precipitation

Monthly and seasonal precipitation is evaluated using two common measures for the overlapping period of PISCOp and reanalysis (1981–2010): bias (mean of reanalysis minus mean of PISCOp) and Spearman correlation rho. For comparison, the finer grid of PISCOp is interpolated to the different reanalyses grids. Evaluation with the station observations is conducted using a distance weighted average of the four closest grid points, as this yields similar results to using the best correlating grid point. We analyse the reanalyses for the rainy season January–February–March (JFM). For comparison purposes, we further use an area mean of the evaluation measures for an area around 12°–16°S and 74°–69°W covering the southern highlands station
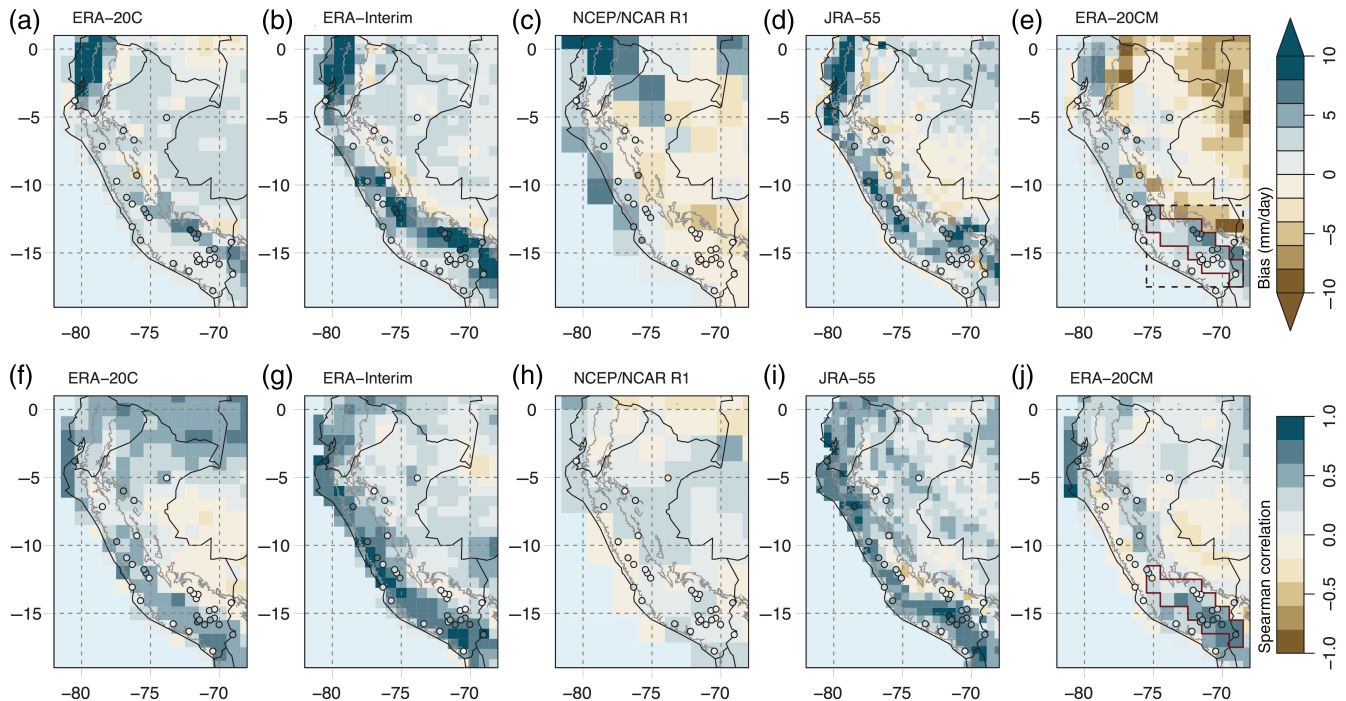
FIGURE 2 Evaluation of JFM precipitation from reanalysis data sets with PISCOp (colours) and stations (circles) for 1981–2010. (a–e) Bias (reanalysis – observations), (f–j) Spearman correlation of precipitation anomalies. 1,000 m a.s.l. shown as grey contour line. The polygon in ERA-20CM depicts the area used for SPI calculations in the composite study. The dashed rectangle depicts the area used for calculating the evaluation metrics of every reanalysis excluding coastal and lowland area [Colour figure can be viewed at wileyonlinelibrary.com]

(dashed box denotes this area in Figure 2). Due to the different grid resolutions, this area varies slightly for every reanalysis.

2.3 | Measures of drought and El Niño

In order to distinguish rainy seasons with droughts and rainy seasons without droughts, we rely on the standardized precipitation index (SPI; McKee et al., 1993; 1995). This index is recommended (in addition to other indices) to national meteorological services for drought monitoring to characterize meteorological droughts due to its simple calculation and effectiveness in describing both dry and wet periods (World Meteorological Organization, 2012). It is based on a transformation of precipitation values to a normal distribution using an equal-probability transformation. We choose a two parameter mixed gamma distribution for precipitation, because this produces good relative fits across different accumulation periods and climatic regions (Stagge et al., 2015). We focus on the 3 months from January to March as this is the period of highest precipitation and important for agricultural production.

For defining moderate meteorological droughts, the two thresholds of −1 or less (−0.84 or less) have been suggested, associated to the non-exceedance probability of .159 (.201) (McKee et al., 1995; Agnew, 2000). The threshold of −1 or less is also recommended in the WMO guidelines for the

SPI droughts (Zargar et al., 2011; World Meteorological Organization, 2012). Based on a drought severity classification, the US National Drought Mitigation Centre reports an SPI value of −0.8 to −1.2 as moderate drought. Their category includes first damage to crops or pastures and is thus interesting for agricultural climate services. For defining droughts in our study, we adopt this threshold of −0.8 or less. This corresponds to a non-exceedance probability of .212. This is reasonable, as impacts of dry conditions may already start earlier than at a threshold of −1 or −0.84. However, specific impacts on agriculture associated with this threshold still need to be evaluated for the southern highlands of Peru. Analyses with other thresholds do not deviate substantially from the here presented results. Sanabria et al. (2018) calculate precipitation anomalies for two different time periods (1964–1977 and 1978–2016) taking into account the climatic shift in the Pacific Ocean during the 1970s (Trenberth and Stepaniak, 2001). We made SPI calculations for the two options using one reference period for 1964–2016 and using two different reference periods as stated above. Here, we only present the results using the reference period 1964–2016 for observations and the reference period 1964–2010 for ERA-20CM.

To define droughts based on observational data, the mean SPI from 16 observational records in the southern Andes of Peru is calculated between 1964 and 2016 using the same period as reference period. All considered stations lie at an

TABLE 2 Selection of El Niño (ENSO+) and La Niña (ENSO−) years for the JRA-55 composite study based on ONI values from ERSSTv4 data for the period 1964–2016 and distinction into CP and EP events

	Drought			No drought		
	Year	ONI	Type	Year	ONI	Type
ENSO+				1973	1.16	EP
	1964	0.56	CP	1977	0.62	EP
	1966	1.04	CP	1995	0.69	CP
	1969	0.95	CP	1998	1.80	EP
	1983	1.80	EP	2003	0.69	CP
	1987	1.19	EP	2005	0.63	CP
	1992	1.51	CP	2010	1.16	CP
	2016	1.99	EP	2015	0.51	CP
ENSO−	1968, 1971, 1974, 1975, 1976, 1985, 1989, 1996, 1999, 2000, 2006, 2008, 2009, 2011, 2012					

elevation above 3,200 m a.s.l. All rainy seasons with a mean 3-monthly SPI in JFM of −0.8 or less are then defined as droughts. This threshold is also reinforced, because the areal mean of the 3-month SPI for JFM only reaches a value of below −1 three times.

To define droughts in the ERA-20CM model simulations, SPI values are calculated as described above with total precipitation for all ERA-20CM members individually (i.e., no observations). We use an area covering the 16 observational records using a reference period from 1964 to 2010 excluding coastal areas and lowlands (red area in Figure 2e).

For the distinction into El Niño events, we rely on established definitions: El Niño events are defined when the ONI (based on 3-monthly running mean SST anomalies in the NIÑO3.4 region) is equal or above 0.5°. We focus on events where this threshold is met during our period of interest, that is, January–March (Table 2). For EP and CP El Niño events, we adopt the "consensus" between different calculation methods evaluated by Yu *et al*. (2012). Using this consensus, we also include events, where the ONI is not equal or above 0.5° in our period of interest and we do not consider the mixed EP/CP type of events.

2.4 | Composite study

Atmospheric conditions during El Niño and drought events are analysed performing two individual composite studies, one using the reanalysis JRA-55 and the second using ERA-20CM ensemble members. In both studies, statistical significance of the differences between the composites is assessed with a Student's *t* test (Wilks, 2011). In the following, we briefly describe the two composite studies.

1. To establish the relationship between El Niño, atmospheric circulation and droughts, we use the JRA-55 reanalysis to make composites of wind and geopotential height (GPH) at 200 hPa for El Niño years with droughts and El Niño years without droughts. JRA-55 covers the full period of observational records and is thus suitable for this purpose. The composites are then based on rainy seasons with an ONI equal or above 0.5°C and a SPI of −0.8 or less. As a reference we make composites of the same variables for El Niño (ONI ≥ 0.5°C) and La Niña (ONI ≤−0.5°C) for the 1964–2016 period irrespective of SPI.

2. To test whether the relationship found is due to the effect of SSTs, we then used the 10 ERA-20CM simulations for the period 1964–2010 (model simulations are only available until 2010). With the model simulations we make composites of wind and GPH at 200 hPa for EP (CP) events with droughts minus EP (CP) events without droughts. SST perturbations within the ERA-20CM members are minor; hence, we use the same EP/CP distinction for all members of the same year. The droughts are defined as stated in section 2.3.

3 | RESULTS AND DISCUSSION

3.1 | Evaluation of reanalysis and model precipitation

Seasonal sums of precipitation (JFM) in the southern Peruvian highlands show a spatial pattern highly influenced by the complex topography of the Andes through orographic processes and low-level winds (Figure 1a; Espinoza *et al*., 2015). This topographic precipitation pattern as it is seen in PISCOp is not fully reflected by the different reanalyses. For the austral summer season, the higher-resolved reanalyses (ERA-Interim, JRA-55 or MERRA) overestimate precipitation along the Andes, mainly along the eastern slopes, but slightly underestimate it in the eastern adjacent lowlands below 1,000 m a.s.l. (Figure 2, upper row and Table 3 for

TABLE 3 Areal mean of RMSE, Spearman correlation and bias for the seven evaluated reanalyses in the area in the southern Peruvian Andes (12°–17°S and 75°–69°W excluding coastal areas and areas in the Amazon basin) for the rainy season JFM

Reanalyses	RMSE (mm/day)	Spearman correlation (rho)	Bias, mm/day (%)
MERRA	1.40	0.17	5.07 (109.80)
ERA-Interim	1.67	0.45	6.27 (128.96)
NCEP/NCAR R1	1.72	0.11	−1.89 (−32.08)
JRA-55	1.27	0.37	3.33 (72.37)
20CRv2c	3.09	0.24	9.91 (168.28)
ERA-20C	1.1	0.35	4.05 (71.54)
CERA-20C (ensemble mean)	1.01	0.35	3.38 (85.77)
ERA20CM (ensemble mean)	0.77	0.39	3.37 (66.37)

area values). This pattern is best visible for MERRA (Figure S1b, Supporting Information) and ERA-Interim and to a lesser degree for JRA-55, whereas NNR does not show such a spatial bias pattern (Figure 2b–d). In our study area, NNR has mostly negative biases, with less precipitation compared to PISCOp and 20CRv2c shows grid cells with biases of above 10 mm/day next to grid cells with biases of –2 mm/day (Figure S1a). For the ensemble mean of ERA-20CM, we find as well high biases along the Andes decreasing towards the west (Figure 2e). Different to ERA-20C, biases in the eastern lowlands (the Amazon basin) are mostly negative. The areal means of the bias for the southern Andes show low values for JRA-55 (3.33 mm/day) and for CERA-20C (3.38 mm/day; Table 3 and Figure S1c). The lowest value is found for NCEP/NCAR R1 (−1.89 mm/day), but its sign is negative. The highest bias is found for 20CRv2c (9.91 mm/day). Excluding NCEP/NCAR R1 and 20CRv2c, biases corresponds to around 70–130% of the mean value of JFM precipitation in PISCOp. ERA-20CM shows a comparatively low bias of 3.37 mm/day (66.37%) and the lowest RMSE (0.77 mm).

Highest positive Spearman correlations between reanalyses and PISCOp are found along the western Andes (Figure 2, lower row) in all data sets except NNR. High correlation values between reanalyses and PISCOp are to some degree congruent with higher correlation values between NIÑO3.4 (or NIÑO1+2) and JFM precipitation for areas that show positive as well as negative correlations with El Niño (Figure 1b). In the eastern highlands, correlation values between reanalyses and PISCOp are drastically decreased, with some areas in ERA-20C, JRA-55, MERRA and ERA-Interim even showing slightly negative correlations (Figures 2, lower row and S1e). Similarly, ERA-20CM

shows higher positive correlations with PISCOp in the Andes compared to the coast and the lowlands, where certain areas even show negative correlations. For most reanalyses, areas with high biases correspond to the areas where correlation values are decreased. For the areal mean of austral summer, highest Spearman correlation is found for ERA-Interim (0.45) and JRA-55 (0.37). The ensemble mean of ERA-20CM shows a correlation of 0.39 with precipitation from PISCOp.

To some extent, monthly values for correlation and bias show different results throughout the course of the year (Figure S2). ERA-Interim, MERRA as well as NNR show higher correlations during winter and summer months, and slightly decreased values during the transition months in spring and autumn. As noted above, JRA-55 performs better during the dry season, that is, the austral winter months, than during the summer months. For RMSE and rho, the two reanalyses ERA-Interim and JRA-55 show the best performance throughout the year. The correlation values between 0.4 and 0.6 are however still rather low for applications, for example for drought monitoring. Regarding the bias, NNR sticks out, as its bias shows the opposite behaviour compared to the other evaluated reanalyses, with overestimation during the dry season and underestimation during the wet season compared to PISCOp. 20CRv2c shows a much higher bias during the rainy season compared to the other reanalyses.

In regions with few assimilated data and in complex topography, precipitation from reanalyses is known to have considerable caveats. Blacutt et al. (2015) conducted an evaluation of precipitation for the Bolivian Andes and found a positive bias for the Andes' eastern facing slopes and negative bias in the lowlands in MERRA and CFSR. They relate this to an insufficient representation of topography in the models for Peru and Bolivia. As topography is very complex and highly variable in the Andes, orographic lifting and precipitation may occur on small spatial scales. Even higher resolved models such as JRA-55 or MERRA cannot reproduce the steep gradients between the Amazon and the Andes, and thus may cause the underestimation and respective overestimation along the Amazon–Andes interface.

Espinoza et al. (2015) identified a rainfall hotspot situated at the eastern flank of the Andes in station observations and TRMM satellite data which is also visible in PISCOp (Figure 1a at 14°S and 70°W). They link this rainfall hotspot to topography–low-level wind interactions, that is, orographic effects of the South American low-level jet, SALLJ. ERA-Interim shows a perpendicular angle between low-level winds at 850 hPa and topography leading to orographic uplifting and rainout. As topography in ERA-Interim (and in other reanalyses) is considerably lower compared to a high-resolution model of topography, the positive bias of ERA-

Interim precipitation (and other reanalyses) on elevations above 1,000 m a.s.l. may come from the uplifting process in the model bringing rain further into the highlands than in reality. According to Espinoza *et al.* (2015), these low-level winds transport moist air towards the mountains in summer and winter, explaining the positive bias in the mountains occurring in both seasons. Chavez and Takahashi (2017) also explain precipitation hotspots along the Amazon–Andes interface, where reanalyses underestimate precipitation compared to PISCOp, with an interaction between topography and the SALLJ, but additionally discuss triggering of convection by downslope winds during night-time. Such effects might not be reproduced properly in reanalyses due to the low resolution and could further contribute to the noted shift in reanalysis' precipitation maximum mountainwards. In conclusion, biases seem mostly related to model resolution and corresponding topography. For the purpose of looking at dry periods in the central Andes using a SPI, a relatively good correlation with observations, which is the case for ERA-20CM, is more important than a small bias.

For various applications in the agricultural or water sector, daily precipitation data are needed and thus an evaluation of daily precipitation data would be crucial. Here, it has been omitted due to the already low performance on monthly basis, but it may be important for new reanalysis products with higher resolutions, which are currently under development.

3.2 | ENSO and drought in the southern Peruvian highlands

3.2.1 | Time series analysis

In the period 1964–2016, eight drought events have been registered for the rainy season months January–March based on the station data from the CPJ area (Figures 3a and S3). Apart from the drought in 1990, all drought events took place during El Niño years. This 1990 drought event with an SPI of −1.13 and thus a rather strong drought can not be related to El Niño, though strong westerly wind anomalies
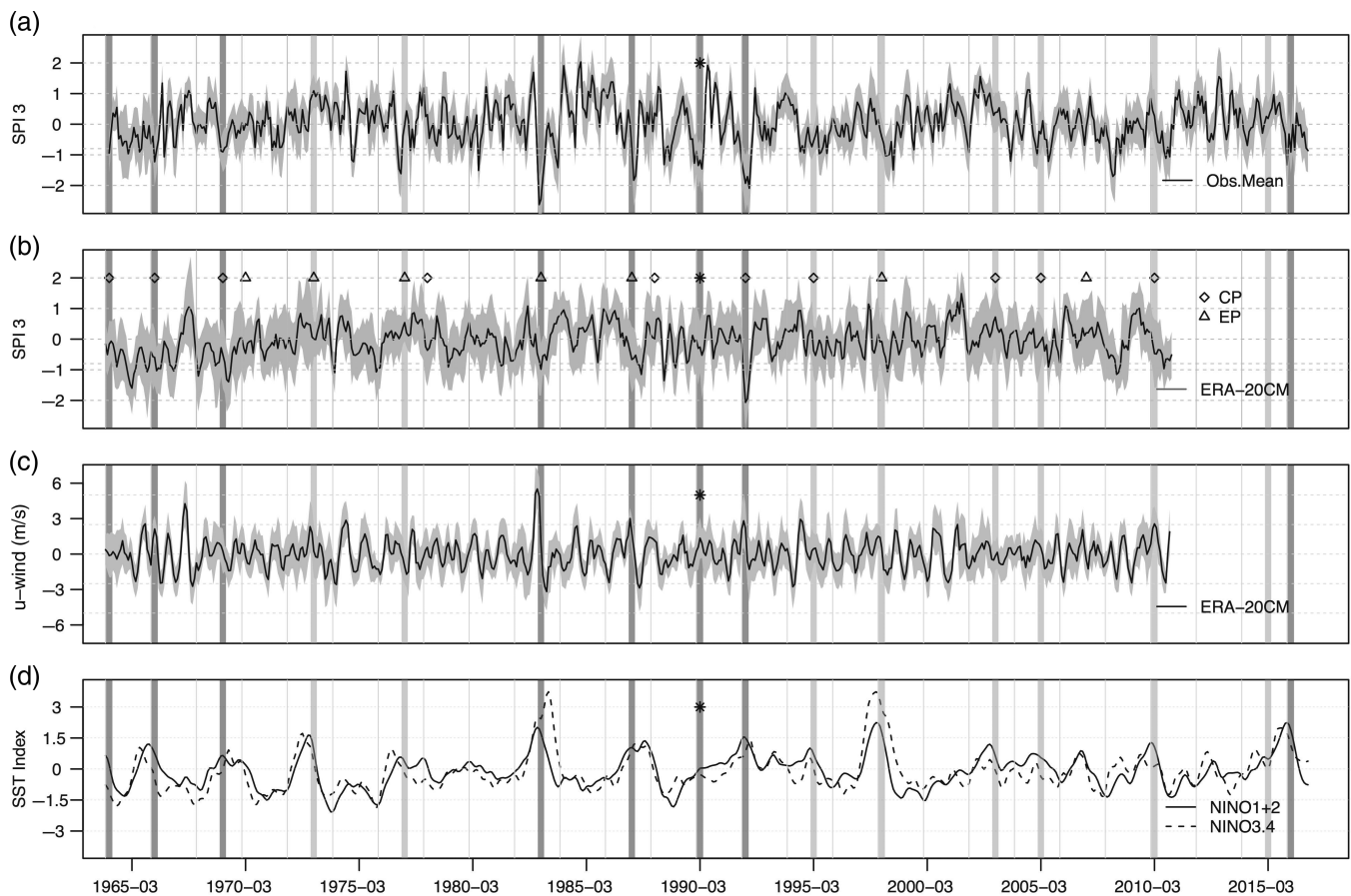
FIGURE 3 (a) Mean 3-monthly SPI time series from station observations for 1964–2016. Grey area represents the spread of the observation data. (b) 3-monthly SPI time series from ERA-20CM ensemble mean and spread (grey area). EP/CP El Niño events for 1964–2010 are marked as triangles/diamonds based on the calculation of Yu *et al.* (2012). (c) Mean and spread of 200-hPa zonal wind anomaly for ERA-20CM for the area 10–19°S and 71°–80°W during 1964–2010. (d) NIÑO1+2 and NIÑO3.4 SST indices. For visual clarity, El Niño events with an ONI ≥ 0.5° in JFM are marked with a darkgrey/lightgrey bar when occurring together with a drought/without a drought. The 1990 drought without El Niño is marked with an asterik. EP/CP events without bars did not show an ONI ≥ 0.5° in JFM

TABLE 4 Contingency table of El Niño and drought events for the period 1964–2016 only looking at the months January–February–March

	Drought	No drought	Total
El Niño	7	8	15
No El Niño	1	22	23
La Niña	0	15	15
Total	8	45	53

are found in the north of the study area. For this event, no drought conditions are registered in the ensemble members of ERA-20CM. The mean is around 0 and the spread is large (Figure 3b). For eight El Niño events during the 1964–2016 period, no drought conditions have been registered (Tables 2 and 4). During the El Niño years 1973, 2003 or 2010, no drought conditions have been registered for the JFM rainy season in the study area, but normal or even above-normal SPI conditions (Figure 3a). During the 1976/1977 and the 2005/2006 El Niño, dry conditions were registered earlier in the rainy season (in OND and NDJ), but as we focus on JFM, these dry conditions are not part of the drought composites. For 5 years, 1970, 1978, 1980, 1988 and 2007 El Niño conditions have been registered with an ONI above 0.5 before JFM (using ERSSTv4); thus, we did not include these years. For the 1997/1998 rainy season, one of the strongest El Niño events of the last century, no drought conditions have been registered. Precipitation was nevertheless below average for the station mean (SPI of −0.34) in the study area. In this year, areas in the lowlands east of the Andes show much below average rainfall for the PISCOp data set (not shown). Calculations splitting the reference period into two parts in order to account for the climatic shift in the Pacific Ocean increases the drought signal (SPI values are lower) in the first few years 1964–1969. SPI values are lower in the three drought rainy seasons 1964, 1966 and 1969. However, no additional rainy season is reaching the threshold of −0.8 and due to the short period (1964–1977) for calculating the SPI, we do not consider these results.

Applying Fisher's exact test to check if the occurrence of El Niño and drought events are independent yields a *p*-value of .0005. This suggests that the two events are not independent. However, again our sample size is very small. The two strongest El Niño drought events happened in 1983 (EP/SPI −2.37) and in 1992 (CP/SPI −1.93) during two different El Niño flavours. In the zonal wind anomalies of ERA-20CM we see a large positive anomaly for both events, as well as for the 1987 drought (Figure 3c). The two droughts in 1983 and 1992, however, both followed a volcanic eruption in the Tropics, the El Chichón in April 1982 in Mexico (17°21′36″N and 93°13′40″W) and Mt. Pinatubo in June 1991 in the Philippines (15°8′0″N, 120°21′0″E). Two

studies found a significant decrease in precipitation after large volcanic eruptions for the Amazon basin and the northern half of the Andes using CMIP-5 and GCM simulations (Iles and Hegerl, 2014; Wegmann et al., 2014). Volcanic eruptions lead to a decrease in global mean precipitation due to a reduction of incoming short-wave radiation and thus, to less evaporation and less condensation in a cooler atmosphere (Iles and Hegerl, 2014). This aspect should not be neglected when looking at the occurrence of drought events in the southern Peruvian Andes.

For the most recent drought event in 2016, SPI values were especially low for January with −1.32 but rose again in the following months (Figure 3a,c). This El Niño has been described as an event in the middle of the continuum between EP and CP events (L'Heureux et al., 2017; Paek et al., 2017). It showed anomalies in NIÑO1+2, but the largest amplitude of SST anomaly were found in the NIÑO3.4 region. None of the more recent and also more frequent CP events since 2000 (McPhaden et al., 2011) have led to moderate to severe droughts.

For our study area in the southern Peruvian highlands, the two ENSO indices (NIÑO3.4 and NIÑO1+2) show areas of significant negative correlation with precipitation values from the PISCOp data set (we did not check for field significance; Figure 1b). Along the western Cordillera of Peru, the correlation with the precipitation sum is more significant for NIÑO3.4 than for NIÑO1+2. The 3-monthly SPI time series from observations correlates slightly stronger with NIÑO3.4 (−0.50) than NIÑO1+2 (−0.42) (Figure 3a,d). For zonal upper-level winds over the Peruvian Andes and precipitation sums, correlation values are at the same order of magnitude or slightly lower: ERA-Interim (−0.47), JRA-55 (−0.41) and ERA-20C (−0.23).

Spearman correlation values between the ensemble mean of the zonal winds from ERA-20CM and precipitation sums reach −0.64, and they reach 0.75 (0.55) for NIÑO3.4 (NIÑO1+2). For the ensemble mean of ERA-20CM, we also calculate a linear regression to check their linear dependence: the two ENSO indices NIÑO3.4 (NIÑO1+2), explain 52.6% (19.8%) of this zonal wind's variability over the central Andes.

Based on station data, Lavado-Casimiro and Espinoza (2014) find a stronger inverse influence of central Pacific SST on summertime precipitation than of eastern Pacific SST. Similarly, Sulca et al. (2017) find precipitation along the western Cordillera of Peru significantly negatively correlated to the C index, which describes SST anomalies in the central Pacific. For the E index, which describes SST anomalies in the eastern Pacific, they find high negative correlations mainly for an area west of Lake Titicaca (Figure 1b). Sulca et al. (2017), however, use an earlier version of the PISCOp data set. In their study, the significant correlations

for the E index in the southern Peruvian Andes become insignificant when the two extreme years 1983 and 1998 are removed.

These studies and our preliminary findings thus reaffirm that El Niño is important, but is also not a sufficient criterion for the occurrence of seasonal precipitation deficits in the southern Peruvian Andes.

3.2.2 | Drought/non-drought composites during El Niño events

In the first composite study encompassing JRA-55 data for 200-hPa winds and GPH, we compared the El Niño situations with droughts and without droughts recorded in station data during the rainy season months January–March.

During El Niño situations, stronger easterly winds prevail over the equator at 200 hPa throughout the Pacific as a result of the reversal of the Walker circulation (Figure 4a). North and south of the equator westerly winds are stronger compared to neutral conditions as they balance the stronger temperature gradients between the Tropics and higher latitudes. The opposite is found for La Niña (Figure 4b). During La Niña, we find an increase in westerly winds compared to neutral conditions along the equator and stronger easterly winds over the central Andes.

The JRA-55 composites for El Niño rainy seasons with droughts and without droughts (Figure 4c,d) both show these typical El Niño conditions over the Pacific Ocean, but they differ noticeably over the central Andes. For drought years, significant upper-level southwesterly wind anomalies are present in a large area over the central Andes, whereas for El Niño years without droughts, winds show no westerly anomaly over the central Andes. Yet, they show a significant northwesterly component south of the central Andes and south of Bolivia towards the southern Atlantic. Throughout the Pacific, polewards from 40°S, El Niño drought years show easterly wind anomalies, whereas for El Niño years without droughts, in this area no explicit pattern is visible. Also, zonal wind anomalies are stronger over the Pacific Ocean for droughts compared to years without droughts.

The GPH field at 200 hPa gives insight into the extent of tropospheric warming during El Niño events. For the El Niño composite, the positive anomaly in the tropical Pacific Ocean with two maxima indicates the position of stationary Rossby waves, forming as a result of increased convective activity over the tropical Pacific (Figure 4e). In the El Niño situations stratified into years with droughts, the GPH anomaly is stronger to the south of the equator, whereas in non-droughts years it is slightly more developed to its north (Figure 4g,h). For the non-drought composites, the positive anomaly in GPH extends more to the southeast compared to the drought composite. Removing the strong 1997/1998 El Niño from the composites does not affect this pattern of southeastwards extended positive GPH (figure not shown). In El Niño years without droughts, the area with significant differences in the GPH fields compared to neutral conditions extends all over the Tropics. Furthermore, for El Niño drought years, a much stronger negative anomaly of the GPH field is found in the southern Pacific between 35°S and 60°S off New Zealand extending towards the western Chilean Coast, compared to years without droughts.

The two composites based on the SPI-3 time series from station observations and the JRA-55 data, however, include a very small number of events; thus, the findings dependent on these composites are not very robust. Nevertheless, the drought composites confirm what has been reported manifold. Stronger westerly wind anomalies over the central Andes have been found to relate to dry conditions on interannual, annual and subseasonal timescales for the Altiplano (e.g., Garreaud and Aceituno, 2001; Garreaud et al., 2003; Vuille and Keimig, 2004) as well as for regions north of the Altiplano, for example, the Mantaro River basin (Sulca et al., 2016). These westerly wind anomalies are related to ENSO through tropospheric warming and the westwards displacement of the Walker circulation. Garreaud and Aceituno (2001) relate the occurrence of dry conditions in the Altiplano to the spatial extent of tropospheric warming. For example, during the El Niño 1972/1973, the tropospheric warming reached around 30°–40°S. Thus, it did not influence the mean climatic flow with easterly winds related to the Bolivian High, and to that effect led to (slightly above) normal rainfall conditions in the Altiplano (Garreaud and Aceituno, 2001).

During drought situations, the pattern found in the southern Pacific resembles the Pacific South American (PSA) pattern as described by Mo and Ghil (1987), especially its first mode (PSA1). The PSA is seen as the Southern Hemisphere response to ENSO in the inter-annual band (Karoly, 1989). Mo and Paegle (2001) showed that during the rainy season of South America, positive events of PSA1 are associated with a predominant pattern of westerly moisture fluxes over the central Andes, which (in comparison with previous studies and our results) is related to drought conditions over this region. Under this premise, it is possible that a high response of the PSA1 during El Niño events is also necessary for causing drought conditions over the southern Peruvian Andes.

3.2.3 | Dry–wet composites during EP and CP El Niño events

The ERA-20CM members stratified into dry (drought) and wet (without drought) conditions allow for a more robust picture and a distinction into EP and CP El Niño, but this
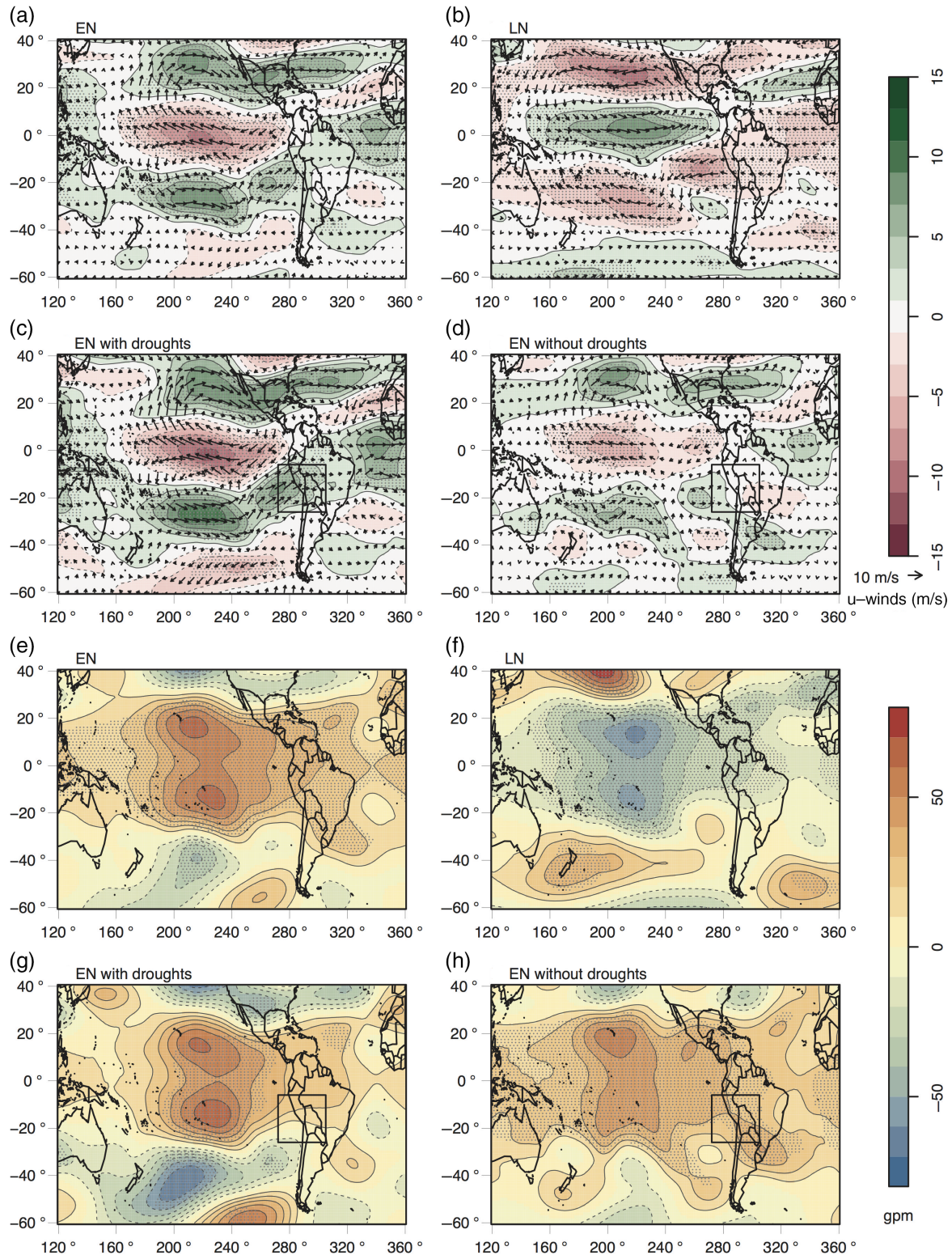
FIGURE 4 JRA-55 composites of 200-hPa winds and GPH based on observed SPI for JFM 1964–2016 with respect to neutral ENSO conditions. Wind anomalies are shown in the top two rows (zonal component coloured) and GPH anomalies are shown in the bottom two rows. El Niño and La Niña conditions are shown in (a, b, e, f). El Niño with and without droughts are shown in (c, g) and (d, h), respectively. Solid/dashed lines indicate positive/negative anomalies. Stippling indicates significant differences at a 95% confidence level. The box marks the study area [Colour figure can be viewed at wileyonlinelibrary.com]

stratification does not reduce the influence of strong events. Based on the calculation of Yu *et al.* (2012), 10 CP and 7 EP El Niño were recorded in the period 1964–2010. Using this classification, the stratification of the ERA-20CM ensemble members into dry (−0.8 or less) and wet members leads to 36 (64) CP members with droughts (without drought) and 17 (53) EP members with droughts (without droughts).

EP events are characterized by positive SST anomalies extending to the very east of the Pacific Ocean (NIÑO1+2 region). Strong easterly wind anomalies are present at 200 hPa along the equator and strong westerly winds to its north and south, respectively. Over the central Andes, we find westerly wind anomalies which are partly recurring southwards when passing the Andes (Figure 5a). CP events show a similar picture but with generally smaller anomalies especially over the central Andes (Figure 5b). In the GPH composites, both EP and CP show the two Rossby waves north and south of the equator in the central Pacific, but the southern Rossby wave is stronger developed in EP (Figure 5e,f).

The two composites for 200-hPa winds stratified into dry–wet EP and CP events resemble the general El Niño events with dry situations related to stronger upper-level easterly anomalies over the equatorial Pacific and, respectively, stronger westerly anomalies to the south and north, in both cases with stronger anomalies for EP (Figure 5c,d). Dry situations show significantly stronger westerly winds over the central Andes up to the northern parts of South America for CP and EP events. To the south of the central Andes, easterly wind anomalies are present in both composites, though only significant in CP.

The dry minus wet composites of GPH show a more variable picture between EP and CP events. During EP events, dry situations in the southern Peruvian Andes are related to a significantly stronger warming of the troposphere in the central Pacific both north and south of the equator and a lower GPH around 40°S (Figure 5g), that is, a stronger temperature gradient in this area. During EP, we find significantly lower values of GPH for dry situations south of the central Andes. During CP events, dry situations show no significant difference in the central Pacific, but they show a significant difference for the surrounding areas, over and to the west of the central Andes, in the Atlantic, and north and west of the central Pacific (Figure 5h). Dry situations during EP events therefore seem to be related to a stronger warming of the troposphere over the central Pacific, that is, the convection over the central Pacific stemming from stronger SST anomalies in the central Pacific.

Regressing a convective index (based on outgoing long-wave radiation) onto the 200-hPa wind field for the Altiplano, Garreaud and Aceituno (2001) found a picture similar

to our dry–wet zonal wind composites with westerly (easterly) flow anomalies in the north (south) over the central Andes. They relate these flow anomalies to seasonal changes in the position and intensity of the Bolivian High. This suggests that our results are consistent with former studies and that they reflect the same changes in the Bolivian High. Sulca *et al.* (2016) found the same anomalous picture using composites of dry spells (3.5–7 days) in the Mantaro River basin located in the north of the CPJ region. They relate these dry spells to a dipole system between the Bolivian High and Nordeste Low, which is sensitive to convective forcing over the Amazon, over the equatorial Atlantic and subtropical Africa, as well as the western Pacific, and to extratropical Rossby wave forcing (Sulca *et al.*, 2016, and references therein).

The resemblance with the PSA pattern (especially with its first mode), we have noted in the GPH during El Niño years with droughts, is as well noticeable in the EP dry–wet composite, but not in the CP composites. Furthermore, the geopotential gradient between the central Pacific and the southern Peruvian Andes is stronger during EP events with droughts, similarly, as it is seen in the El Niño–drought composites. Thus, it seems that EP events with both of these features, a PSA1 and the high geopotential gradient over the region are important for leading to stronger westerly wind anomalies and, therefore, to drought conditions. The positive GPH anomalies for dry–wet EP events also suggest that stronger EP events (possessing also strong SST anomalies in the central Pacific) are related to drier conditions in the Andes. For CP events, we cannot identify such patterns.

Interestingly, in the GPH composite of EP dry–wet, an area located at the southern tip of the climatological position of the SPCZ shows an increased north–south gradient during dry events in the southern Peruvian Andes compared to wet events (Figure 5g). Some studies have linked the SPCZ to precipitation deficits during the rainy season in the central Andes (Garreaud and Aceituno, 2001; Vuille and Keimig, 2004), and also on subseasonal timescales (Sulca *et al.*, 2016). Sulca *et al.* (2017) found a northwards displacement of the SPCZ to be related to less precipitation over the southern Andes of Peru. ENSO leads to a north and eastwards displacement of the SPCZ with a more zonal component, or even to a collapse to a zonal band during strong ENSO events (1982–1983, 1991–1992, 1997–1998; van der Wiel *et al.*, 2016).

Classifying El Niño into EP or CP is, however, not for every event straight forwards and may depend on the chosen methodology (Capotondi *et al.*, 2015). Certain events are classified as mix-typed El Niño as the indices based on the SST anomalies indicate both. The 2015/2016 El Niño, considered as an extreme El Niño similarly to 1997/1998, caused drought conditions in our study area, whereas during the
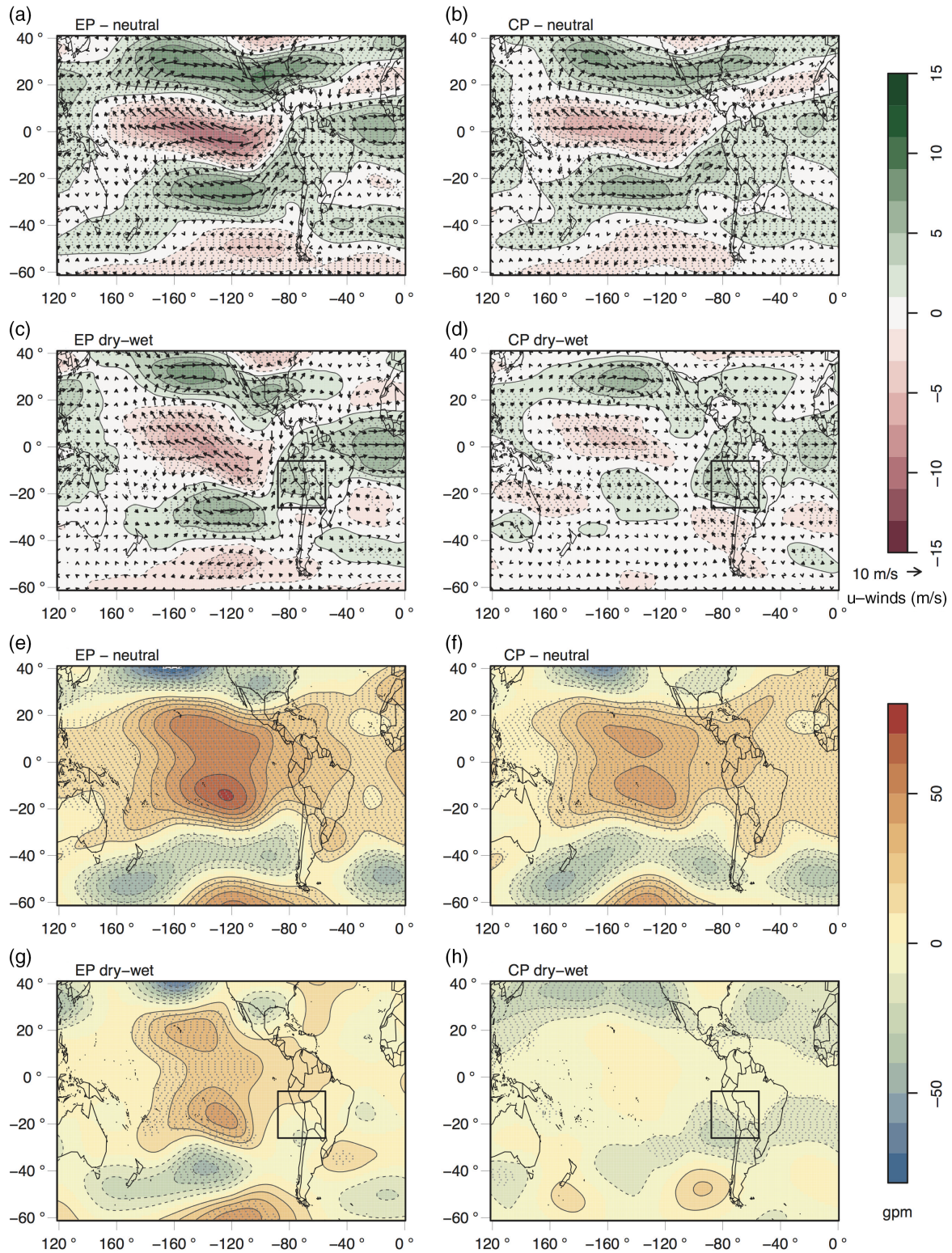
FIGURE 5 ERA-20CM composites of 200-hPa winds and GPH based on ERA-20CM SPI for JFM 1964–2010. Wind anomalies are shown in the top two rows (zonal component coloured) and GPH anomalies are shown in the bottom two rows. EP and CP conditions with respect to neutral conditions are shown in (a, b, e, f). EP and CP dry–wet conditions are shown in (c, g) and (d, h), respectively. Solid/dashed lines indicate positive/negative anomalies. Stippling indicates significant differences at a 95% confidence level. The box marks the study area [Colour figure can be viewed at wileyonlinelibrary.com]

1997/1998 El Niño, only slightly drier-than-normal conditions were recorded. A comparison study on these two strong El Niño events showed that the 1997/1998 event followed the pure EP El Niño dynamics, whereas in the decaying stage the 2015/2016 event also involved CP dynamics (with higher SST anomalies around the date line) which depend on subtropical forcing (L'Heureux *et al*., 2017; Paek *et al*., 2017). A lot of studies have been conducted on the different effects and teleconnections of EP and CP El Niño (e.g., Kao and Yu, 2009; Yu *et al*., 2012; Tedeschi *et al*., 2013; Alizadeh-Choobari, 2017), but the processes behind the different SST anomalies are still not fully clear. Mayer *et al*. (2013) consider the CP El Niño (El Niño Modoki) as part of the ENSO evolution and as a transition state between cold and warm phases and not as two distinct types. Capotondi *et al*. (2015) summarize the diversity of ENSO events as being neither solely EP or CP but as linear combination of both ENSO flavours. This should be kept in mind, when analysing the atmospheric conditions leading to droughts for EP and CP events.

4 | CONCLUSION

Our study examines two aspects of precipitation and precipitation deficits in the southern Andes of Peru: the representation of precipitation in reanalyses data sets and the relationship between El Niño, zonal wind anomalies and precipitation deficits. Seasonal (JFM) precipitation from reanalyses for Peru show high spatial differences in their representation of inter-annual variability and mean values of precipitation. In the austral summer season, the higher-resolved reanalyses overestimate precipitation along the Andes, mainly the eastern facing slopes, but slightly underestimate it in the eastern adjacent lowlands (Figure 2, upper row). This may stem from the simplified topography in the reanalyses that does not hinder moisture flux towards the Andes, producing underestimation on the Andes' eastern facing slopes (below 1,000 m a.s.l.) and overestimation of precipitation on the eastern facing slopes above 1,000 m a.s.l. relative to PISCOp. Correlation values between the different reanalyses and PISCOp are, for most reanalyses, higher along the western part of the Andes and for the northern coastal region of Peru. Overall, the widely applied NNR reanalysis shows a very low performance and is not recommended for use in precipitation studies. In terms of correlation, the best performing reanalyses are ERA-Interim and JRA-55 for both rainy seasons.

Drought events recorded by station data develop during El Niño events, but an El Niño does not necessarily lead to drought conditions. In our time series, droughts occur during central Pacific and eastern Pacific El Niño events and the drought event in 1990 also occurs, while no El Niño was registered. Strong El Niño events do not always coincide with a strong drought, illustrated by the example of the 1997/1998 El Niño without a drought. The rainy season 1982/1983 stands out as it is the major drought of the last century since 1964 with strong zonal wind anomalies over the central Andes. But, the two particularly strong droughts in 1983 and 1992 followed the two major volcanic eruptions of El Chichón and Mt. Pinatubo. As shown by Iles and Hegerl (2014) and Wegmann *et al*. (2014), major volcanic eruptions lead to precipitation deficits over the central Andes.

The composites formed from a small sample of seven droughts confirm the relationship between 200-hPa westerly wind anomalies during El Niño events and precipitation deficits known for the Altiplano of Peru and Bolivia.

In order to evaluate the difference between central Pacific (CP) and eastern Pacific (EP) El Niño events, we rely on the ERA20CM model simulations. For EP events, we find significant differences in the GPH fields at 200 hPa in the tropical central Pacific, if we compare dry and wet situations. Stronger developed Rossby waves in the central Pacific (around 140°W) during EP lead to a stronger gradient towards the southeast and increased upper-level winds. In addition, we found a resemblance to a PSA1 for EP dry events. These two ingredients we consider important for the development of upper-level westerly wind anomalies and thus drought conditions in the southern Andes of Peru.

For an improved understanding of drought occurrence, further research is needed. In order to better understand drought impacts on agriculture, studies are needed that evaluate drought indices and suitable thresholds thereof. Concerning the understanding of drought mechanisms, on the one hand, it is important to focus on moisture transport towards the area and possible relationships to extratropical and Atlantic forcing. On the other hand, further insights may be gained, looking at the temporal evolution of SST anomalies (and their location in the Pacific) and their relationship to droughts.

ORCID

Noemi Imfeld https://orcid.org/0000-0002-9645-6875
Stefanie Gubler https://orcid.org/0000-0002-3733-953X

REFERENCES

Agnew, C.T. (2000) Using the SPI to identify drought. *Drought Network News*, 12, 6–12.

Alizadeh-Choobari, O. (2017) Contrasting global teleconnection features of the eastern Pacific and central Pacific El Niño events, dynamics of atmospheres and oceans. *Dynamics of Atmospheres and Oceans*, 80, 139–154. https://doi.org/10.1016/j.dynatmoce.2017.10.004.

Andreoli, R.V., Soares de Oliveira, S., Kayano, M.T., Viegas, J., Ferreira de Souza, R.A. and Candidio, L.A. (2017) The influence of different El Niño types on the South American rainfall. *International Journal of Climatology*, 37, 1374–1390. https://doi.org/10.1002/joc.4783.

Aybar, C., Lavado-Casimiro, W., Huerta, A., Fernández, C., Vega, F., Sabino, E. and Felipe-Obando, O. (2017) Uso del Producto Grillado "PISCOP" de precipitación en Estudios. In: *Investigaciones y Sistemas Operacionales de Monitoreo y Pronóstico Hidrometeorológico*. Lima: SENAMHI. Nota Técnica 001 SENAMHI-DHI-2017.

Blacutt, L.A., Herdies, D.L., Gonales, L., Vila, D. and Andrade, M. (2015) Precipitation comparison for the CFSR, MERRA, TRMM3b42 and combined scheme datasets in Bolivia. *Atmospheric Research*, 163, 117–131. https://doi.org/10.1016/j.atmosres.2015.02.002.

Capotondi, A., Wittenberg, A., Newman, M., Di Lorenzo, E., Yu, J., Braconnot, P., Cole, J., Dewitte, B., Giese, B., Guilyardi, E., Jin, F. F., Karnauskas, K., Kirtman, B., Lee, T., Schneider, N., Xue, Y. and Yeh, S. (2015) Understanding ENSO diversity. *Bulletin of the American Meteorological Society*, 96(6), 921–938. https://doi.org/10.1175/BAMS-D-13-00117.1.

Chavez, S.P. and Takahashi, K. (2017) Orographic rainfall hotspots in the Andes–Amazon transition according to the TRMM precipitation radar and in situ data. *Geophysical Research Atmospheres*, 122, 5870–5882. https://doi.org/10.1002/2016JD026282.

Compo, G.P., Whitaker, J.S., Sardeshmukh, P.D., Matsui, N., Allan, R. J., Yin, X., Gleason, B.E., Vose, R.S., Rutledge, G., Bessemoulin, P., Brönnimann, S., Brunet, M., Crouthamel, R.I., Grant, A.N., Groisman, P.Y., Jones, P.D., Kruk, M.C., Kruger, A. C., Marshall, G.J., Maugeri, M., Mok, H.Y., Nordli, Ø., Ross, T.F., Trigo, R.M., Wang, X.L., Woodruff, S.D. and Worley, S.J. (2011) The twentieth century reanalysis project. *Quarterly Journal of the Royal Meteorological Society*, 137, 1–28. https://doi.org/10.1002/qj.776.

De Boisséson, E., Balmaseda, M.A., Abdalla, S., Källén, E. and Janssen, P.A.E.M. (2014) How robust is the recent strengthening of the tropical Pacific trade winds? *Geophysical Research Letters*, 41, 4398–4405. https://doi.org/10.1002/2014GL060257.

Dee, D.P., Uppala, S.M., Simmons, A.J., Berrisford, P., Poli, P., Kobayashi, S., Andrae, U., Balmaseda, M.A., Balsamo, G., Bauer, P., Bechtold, P., Beljaars, A.C.M., van de Berg, L., Bidlot, J., Bormann, N., Delsol, C., Dragani, R., Fuentes, M., Geer, A.J., Haimberger, L., Healy, S.B., Hersbach, H., Hólm, E.V., Isaksen, L., Kållberg, P., Köhler, M., Matricardi, M., McNally, A.

P., Monge-Sanz, B.M., Morcrette, J.-J., Park, B.-K., Peubey, C., de Rosnay, P., Tavolato, C., Thépaut, J.-N. and Vitart, F. (2011) The ERA-Interim reanalysis: configuration and performance of the data assimilation system. *Quarterly Journal of the Royal Meteorological Society*, 137, 553–597. https://doi.org/10.1002/qj.828.

Diro, G., Grimes, D., Black, E., O'Neill, A. and Pardo-Iguzaquiza, E. (2009) Evaluation of rainfall estimates over Ethiopia. *International Journal of Climatology*, 29, 67–78. https://doi.org/10.1002/joc.1699.

England, M.H., McGregor, S., Spence, P., Meehl, G.A., Timmermann, A., Cai, W., Gupta, A.S., McPhaden, M.J., Purich, A. and Santoso, A. (2014) Recent intensification of wind-driven circulation in the Pacific and the ongoing warming hiatus. *Nature Climate Change*, 4, 222–227. https://doi.org/10.1038/nclimate2106.

Espinoza, J., Chavez, S., Ronchai, J., Junquas, C., Takahashi, K. and Lavado, W. (2015) Rainfall hotspots over the southern tropical Andes: spatial distribution, rainfall intensity, and relations with large-scale atmospheric circulation. *Water Resources Research*, 51, 3459–3475. https://doi.org/10.1002/2014WR016273.

Falvey, M. and Garreaud, R. (2005) Moisture variability over the South American Altiplano during the South American Low Level Jet Experiment (SALLJEX) observing season. *Journal of Geophysical Research: Atmospheres*, 110(D22), D22105. https://doi.org/10.1029/2005JD006152.

Funk, C., Peterson, P., Landsfeld, M., Pedreros, D., Verdin, J., Shukla, S., Husak, G., Rowland, J., Harrison, L., Hoell, A. and Michaelsen, J. (2015) The climate hazards infrared precipitation with stations—a new environmental record for monitoring extremes. *Scientific Data*, 2, 150066. https://doi.org/10.1038/sdata.2015.66.

Garreaud, R. (1999) Multiscale analysis of the summertime precipitation over the central Andes. *Monthly Weather Review*, 127(5), 901–921. https://doi.org/10.1175/1520-0493(1999)127<0901:MAOTSP>2.0.CO;2.

Garreaud, R., Vuille, M. and Clement, A.C. (2003) The climate of the Altiplano: observed current conditions and mechanisms of past changes. *Paleogeography, Paleoclimatology, Paleoecology*, 194, 5–22. https://doi.org/10.1016/S0031-0182(03)00269-4.

Garreaud, R.D. (2009) The Andes climate and weather. *Advances in Geosciences*, 7, 1–9.

Garreaud, R.D. and Aceituno, P. (2001) Interannual rainfall variability over the South America Altiplano. *Journal of Climate*, 14, 2779–2789. https://doi.org/10.1175/1520-0442(2001)014<2779:IRVOTS>2.0.CO;2.

Hegerl, G.C., Brönnimann, S., Schurer, A. and Cowan, T. (2018) The early 20th century warming: anomalies, causes, and consequences. *WIREs: Climate Change*, 9, e522. https://doi.org/10.1002/wcc.522.

Hersbach, H., Peubey, C., Simmons, A., Berrisford, P., Poli, P. and Dee, D. (2015) ERA20CM: a twentieth-century atmospheric model ensemble. *Quarterly Journal of the Royal Meteorological Society*, 141, 2350–2375. https://doi.org/10.1002/qj.2528.

Hu, X., Yang, S. and Cai, M. (2016) Contrasting the eastern Pacific El Niño and the central Pacific El Niño: process-based feedback attribution. *Climate Dynamics*, 47(7–8), 2413–2424. https://doi.org/10.1007/s00382-015-2971-9.

Huang, B., Banzon, V.F., Freeman, E., Lawrimore, J., Liu, W., Peterson, T.C., Smith, T.M., Thorne, P.W., Woodruff, S.D. and Zhang, H. (2015) Extended Reconstructed Sea Surface

Temperature Version 4 (ERSST.v4). Part I: upgrades and Intercomparisons. *Journal of Climate*, 28, 911–930. https://doi.org/10.1175/JCLI-D-14-00006.1.

Iles, E. and Hegerl, G.C. (2014) The global precipitation response to volcanic eruptions in the CMIP5 models. *Environmental Research Letters*, 9, 104012. https://doi.org/10.1088/1748-9326/9/10/104012.

Kalnay, E., Kanamitsu, M., Kistler, R., Collins, W., Deaven, D., Gandin, L., Iredell, M., Saha, S., White, G., Woollen, J., Zhu, Y., Leetmaa, A. and Reynolds, R. (1996) The NCEP/NCAR 40-year reanalysis project. *Bulletin of the American Meteorological Society*, 77, 437–471. https://doi.org/10.1175/1520-0477(1996)077<0437:TNYRP>2.0.CO;2.

Kao, H. and Yu, J. (2009) Contrasting eastern-Pacific and central-Pacific types of ENSO. *Journal of Climate*, 22, 615–632. https://doi.org/10.1175/2008JCLI2309.1.

Karoly, D.J. (1989) Southern Hemisphere circulation features associated with El Niño–Southern Oscillation events. *Journal of Climate*, 2, 1239–1252. https://doi.org/10.1175/1520-0442(1989)002<1239:SHCFAW>2.0.CO;2.

Kobayashi, S., Ota, Y. and Harada, Y. (2015) The JRA-55 reanalysis: general specifications and basic characteristics. *Journal of Meteorological Society of Japan*, 93, 5–48. https://doi.org/10.2151/jmsj.2015-001.

Lagos, P., Silva, Y., Nickl, E. and Mosquera, K. (2008) El Niño related precipitation variability in Peru. *Advances in Geosciences*, 14, 231–237. https://doi.org/10.5194/adgeo-14-231-2008.

Laloyaux, P., de Boisseson, E., Balmaseda, M., Bidlot, J.-R., Brönnimann, S., Buizza, R., Dalhgren, P., Dee, D., Haimberger, L., Hersbach, H., Kosaka, Y., Martin, M., Poli, P., Rayner, N., Rustemeier, E. and Schepers, D. (2018) CERA-20C: a coupled reanalysis of the twentieth century. *Journal of Advances in Modeling Earth Systems*, 10, 1172–1195. https://doi.org/10.1029/2018MS001273.

Lavado-Casimiro, W. and Espinoza, J. (2014) Impactos de El Niño y la Niña en las lluvias del Peru (1965-2007). *Revista Brasileira de Meteorolgia*, 29, 171–182. https://doi.org/10.1590/S0102-77862014000200003.

Lenters, J.D. and Cook, K.H. (1999) Summertime precipitation variability over South America: role of large-scale circulation. *Monthly Weather Review*, 127(3), 409–431. https://doi.org/10.1175/1520-0493(1999)127<0409:SPVOSA>2.0.CO;2.

L'Heureux, M.L., Takahashi, K., Watkins, A.B., Barnston, A.G., Becker, E.J., Di Liberto, T.E., Gamble, F., Gottschalck, J., Halpert, M.S., Huang, B., Mosquera-Vásquez, K. and Wittenberg, A.T. (2017) Observing and Predicting the 2015/16 El Niño. *Bulletin of the American Meteorological Society*, 98, 1363–1382. https://doi.org/10.1175/BAMS-D-16-0009.1.

McKee, T.B., Doesken, N.J. and Kleist, J. (1993) The relationship of drought frequency and duration to time scale. In: *Proceedings of the Eighth Conference on Applied Climatology*. Boston, MA: American Meteorological Society, pp. 179–184.

McKee, T.B., Doesken, N.J. and Kleist, J. (1995) Drought monitoring with multiple time scales. In: *Proceedings of the Ninth Conference on Applied Climatology*. Boston, MA: American Meteorological Society, pp. 233–236.

McPhaden, M.J., Lee, T. and McClurg, D. (2011) El Niño and its relationship to changing background conditions in the tropical Pacific Ocean. *Geophysical Research Letters*, 38, L15709. https://doi.org/10.1029/2011GL048275.

Mayer, M., Trenberth, K.E., Haimberger, L. and Fasullo, J.T. (2013) The response of tropical atmospheric energy budgets to ENSO. *Journal of Climate*, 26, 4710–4724. https://doi.org/10.1175/JCLI-D-12-00681.1.

Minvielle, M. and Garreaud, R.D. (2011) Projecting rainfall changes over the South American Altiplano. *Journal of Climate*, 24, 4577–4583. https://doi.org/10.1175/JCLI-D-11-00051.1.

Mo, K.C. and Ghil, M. (1987) Statistics and dynamics of persistent anomalies. *Journal of the Atmospheric Sciences*, 44, 877–901. https://doi.org/10.1175/1520-0469(1987)044<0877:SADOPA>2.0.CO;2.

Mo, K.C. and Paegle, J.N. (2001) The Pacific-South American modes and their downstream effects. *International Journal of Climatology*, 21, 1211–1229. https://doi.org/10.1002/joc.685.

Morales, M.S., Christie, D.A., Villalba, R., Argollo, J., Pacajes, J., Silva, J.S., Alvarez, C.A., Llancabure, J.C. and Soliz Gamboa, C.C. (2012) Precipitation changes in the South American Altiplano since 1300 AD reconstructed by tree-rings. *Climate of the Past*, 8, 653–666. https://doi.org/10.5194/cp-8-653-2012.

Neukom, R., Rohrer, M., Calanca, P., Salzmann, N., Huggel, C., Acua, D., Christie, D.A. and Morales, M.S. (2015) Facing unprecedented drying of the central Andes? Precipitation variability over the period ad 1000–2100. *Environmental Research Letters*, 10, 084017. https://doi.org/10.1088/1748-9326/10/8/084017.

Paek, H., Yu, J.-Y. and Qian, C. (2017) Why were the 2015/2016 and 1997/1998 extreme El Niños different? *Geophysical Research Letters*, 44, 1848–1856. https://doi.org/10.1002/2016GL071515.

Perry, L.B., Seimon, A. and Kelly, G.M. (2014) Precipitation delivery in the tropical high Andes of southern Peru: new findings and paleoclimatic implications. *International Journal of Climatology*, 34, 197–215. https://doi.org/10.1002/joc.3679.

Poli, P., Hersbach, H. and Dee, D.P. (2016) ERA-20C: an atmospheric reanalysis of the twentieth century. *Journal of Climate*, 29, 4083–4097. https://doi.org/10.1175/JCLI-D-15-0556.1.

Rayner, N.A., Parker, D.E., Horton, E.B., Folland, C.K., Alexander, L.V., Rowell, D.P., Kent, E.C. and Kaplan, A. (2003) Global analyses of sea surface temperature, sea ice, and night marine air temperature since the late nineteenth century. *Journal of Geophysical Research*, 108(D14), 4407. https://doi.org/10.1029/2002JD002670.

Rienecker, M., Suarez, M., Gelaro, R., Todling, R., Bacmeister, J., Liu, E., Bosilovich, M. and Schubert, S. (2011) MERRA: NASA's modern-era retrospective analysis for research and applications. *Journal of Climate*, 24, 3624–3648. https://doi.org/10.1175/JCLI-D-11-00015.1.

Rosas, G., Gubler, S., Oria, C., Acuña, D., Avalos, G., Begert, M., Castillo, E., Croci-Maspoli, M., Cubas, F., Dapozzo, M., Díaz, A., van Geijtenbeek, D., Jacques, M., Konzelmann, T., Lavado, W., Matos, A., Mauchle, F., Rohrer, M., Rossa, A., Scherrer, S.C., Valdez, M., Valverde, M., Villar, G. and Villegas, E. (2016) Towards implementing climate services in Peru—the project CLIMANDES. *Climate Services*, 4, 30–41. https://doi.org/10.1016/j.cliser.2016.10.001.

Sanabria, J., Bourrel, L., Dewitte, B., Frappart, F., Rau, P., Solis, O. and Labat, D. (2018) Rainfall along the coast of Peru during strong El Niño events. *International Journal of Climatology*, 38, 1737–1747. https://doi.org/10.1002/joc.5292.

Seiler, C., Hutjes, R.W. and Kabat, P. (2013) Climate variability and trends in Bolivia. *Journal of Applied Meteorology and Climatology*, 52, 130–146. https://doi.org/10.1175/JAMC-D-12-0105.1.

Stagge, J., Tallaksen, L., Gudmundsson, L., Van Loon, A. and Stahl, K. (2015) Candidate distributions of climatological drought. *International Journal of Climatology*, 35, 4027–4040. https://doi.org/10.1002/joc.4267.

Sulca, J., Takahashi, K., Espinoza, J., Vuille, M. and Lavado-Casimiro, W. (2017) Impacts of different ENSO flavors and tropical Pacific convection variability (ITCZ, SPCZ) on austral summer rainfall in South America, with a focus on Peru. *International Journal of Climatology*, 38, 420–435. https://doi.org/10.1002/joc.5185.

Sulca, J., Vuille, M., Silva, Y. and Takahashi, K. (2016) Teleconnections between the Peruvian central Andes and northeast Brazil during extreme rainfall events in austral summer. *Journal of Hydrometeorology*, 17(2), 499–515. https://doi.org/10.1175/JHM-D-15-0034.1.

Tedeschi, R., Cavalcanti, I. and Grimm, A. (2013) Influence of two types of ENSO on South American precipitation. *International Journal of Climatology*, 33, 1382–1400. https://doi.org/10.1002/joc.3519.

Tedeschi, R. and Collins, M. (2016) The influence of ENSO on South American precipitation during austral summer and autumn in observations and models. *International Journal of Climatology*, 36, 618–635. https://doi.org/10.1002/joc.4371.

Thibeault, J., Seth, A. and Wang, G. (2011) Mechanisms of summertime precipitation variability in the Bolivian Altiplano: present and future. *International Journal of Climatology*, 32, 2033–2041. https://doi.org/10.1002/joc.2424.

Titchner, H.A. and Rayner, N.A. (2014) The Met Office Hadley Center sea ice and sea surface temperature data set, version 2: sea ice concentrations. *Journal of Geophysical Research: Atmospheres*, 119 (6), 2864–2889. https://doi.org/10.1002/2013JD020316.

Trenberth, K.E. and Stepaniak, D.P. (2001) Indices of El Niño evolution. *Journal of Climate*, 14, 1697–1701. https://doi.org/10.1175/15200442(2001)014<1697:LIOENO>2.0.CO;2.

van der Wiel, K., Matthews, A., Joshi, M. and Stevens, D. (2016) Why the South Pacific Convergence Zone is diagonal. *Climate Dynamics*, 46, 1683–1698. https://doi.org/10.1007/s00382-015-2668-0.

Vuille, M. (1999) Atmospheric circulation over the Bolivian Altiplano during dry and wet periods and extreme phases of the Southern Oscillation. *International Journal of Climatology*, 19, 1579–1600. https://doi.org/10.1002/(SICI)1097-0088(19991130)19:14<1579::AID-JOC441>3.0.CO;2-N.

Vuille, M. and Keimig, F. (2004) Interannual variability of summertime convective cloudiness and precipitation in the central Andes derived from ISCCP-B3 data. *Journal of Climate*, 17, 3334–3348. https://doi.org/10.1175/1520-0442(2004)017<3334:IVOSCC>2.0.CO;2.

Wegmann, M., Brönnimann, S., Bhend, J., Franke, J., Folini, D., Wild, M. and Luterbacher, J. (2014) Volcanic influence on European summer precipitation through monsoons: possible cause for years without summer. *Journal of Climate*, 27(10), 3683–3691. https://doi.org/10.1175/JCLI-D-13-00524.1.

Wilks, S. (2011) *Statistical methods in the Atmospheric Sciences*, 3rd edition. Oxford, UK and Waltham, MA: Academic Press.

World Meteorological Organization. (2012) *Standardized Precipitation Index User Guide*. Geneva: World Meteorological Organization. WMO-No. 1090.

Yu, J., Zou, Y., Kim, S. and Lee, T. (2012) The changing impact of El Niño on US winter temperatures. *Geophysical Research Letters*, 39, L15702. https://doi.org/10.1029/2012GL052483.

Zargar, A., Sadiq, R., Bahman, N. and Khan, F. (2011) A review of drought indices. *Environmental Reviews*, 19, 333–349. https://doi.org/10.1139/a11-013.

SUPPORTING INFORMATION

Additional supporting information may be found online in the Supporting Information section at the end of this article.